Emergent Kondo Behavior from Gauge Fluctuations in Spin Liquids

Rui Wang,[1,2,*] Yilin Wang,[3] Y. X. Zhao,[1,2] and Baigeng Wang[1,2,†]

[1]*National Laboratory of Solid State Microstructures and Department of Physics, Nanjing University, Nanjing 210093, China*
[2]*Collaborative Innovation Center for Advanced Microstructures, Nanjing 210093, China*
[3]*Hefei National Laboratory for Physical Sciences at Microscale, University of Science and Technology of China,*
Hefei, Anhui 230026, China

The Kondo effect is a prominent quantum phenomenon describing the many-body screening of a local magnetic impurity. Here, we reveal a new type of nonmagnetic Kondo behavior generated by gauge fluctuations in strongly correlated baths. We show that a nonmagnetic bond defect not only introduces the potential scattering but also locally enhances the gauge fluctuations. The local gauge fluctuations further mediate a pseudospin exchange interaction that produces an asymmetric Kondo fixed point in low energy. The gauge-fluctuation-induced Kondo phenomena do not exhibit the characteristic resistivity behavior of the conventional Kondo effect, but display a nonmonotonous temperature dependence of thermal conductivity as well as an anisotropic pseudospin correlation. Moreover, with its origin from gauge fluctuations, the Kondo features can be regarded as promising indicators for identifying quantum spin liquids. Our work advances fundamental knowledge of novel Kondo phenomena in strongly correlated systems, which have no counterparts in thermal baths within the single-particle description.

DOI: 10.1103/PhysRevLett.127.237202

Introduction.—The Kondo problem, which treats a magnetic impurity in metals [1], is of key importance in material science, as its solution by renormalization group (RG) [2] and Bethe ansatz [3] invokes some of the most profound concepts and techniques in theoretical physics [4]. When a magnetic impurity is coupled to bath electrons, the magnetic scattering becomes essential and drives a many-body resonance. The Kondo singlet is then formed, displaying the Fermi liquid behavior [5]. In this Letter, we shall extend the scope of Kondo physics to a new avenue, namely, describing bond defects in quantum spin liquids (QSLs).

QSLs are exotic states of strongly correlated and frustrated systems in two dimensions and have constituted one of the most active fields over the last decades [6,7]. Because of strong quantum fluctuation, various QSLs can be stabilized, displaying the fractionalized excitations and emergent gauge field, such as the resonating valence bond states [8] and the flux phases [9–12]. The gauge fluctuations are the most crucial degrees of freedom reflecting the nature of QSLs. They can not only ensure the disordered nature of the deconfined mean-field states [13], but can also generate anyonic excitations via statistical transmutations [14].

Because of the emergent gauge fluctuations, the impurity problems in QSLs are complicated and thus have not been deeply investigated [15,16]. Indeed, there are many important questions to be answered, even if a nonmagnetic defect is considered. For example, is there any nontrivial interplay between the defect and the gauge fluctuations? Moreover, will any novel many-body resonances take place, as a result of the gauge fluctuations?

In this Letter, we reveal novel Kondo signatures of a *nonmagnetic* defect driven by gauge fluctuations in flux phases. The flux phases, which describe effective fermions moving under flux [10], have been extensively studied in the last decades. They were proposed to enjoy intimate connections with several fundamental topics, including the deconfined quantum criticality [17,18], QSLs [19,20], and high-T_c superconductivity [21]. Here, we unveil salient features of a bond defect in the renowned flux phases. We find that the defect not only introduces the potential scattering but also locally enhances the gauge fluctuations, as shown by Fig. 1(a). The gauge fluctuations are able to mediate fermion-fermion interactions. Here, a pseudospin exchange term between the defect and the bath is locally induced. This leads to a low-energy effective theory formally similar to the Kondo problems in Dirac semimetals or graphene [22–29], but with several key distinctions. Particularly, the pseudospin exchange interaction is found to be highly anisotropic and occurs simultaneously with the potential scattering. These distinct features result in an asymmetric Kondo (AK) fixed point. Consequently, a pseudospin Kondo singlet is generated in low energy with new Kondo features, as shown by Fig. 1(b). In sharp contrast with the Kondo effect in normal metals, here we predict a nonmonotonous temperature dependence of thermal conductivity as well as an anisotropic pseudospin correlation.

Our work discovers a new mechanism for Kondo behavior in strongly correlated baths. It implies that the
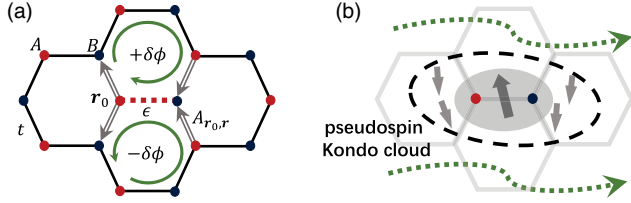
FIG. 1. Demonstration of the gauge field-induced Kondo physics on honeycomb lattice. (a) A bond defect (the dashed line) with quenched local hopping $t_{\mathbf{r}_0 A, \mathbf{r}_0 B} = \epsilon < t$ is considered on top of the flux phase, where t is the nearest-neighbor hopping. For $\epsilon \to 0$, the two hexagons adjacent to the quenched bond become connected, forming a doubled plaquette. Opposite fluctuations, $+\delta\phi$ and $-\delta\phi$, are enabled in the two hexagons, which can be equivalently represented by the local gauge terms $A_{\mathbf{r}_0, \mathbf{r}}$ on the four bonds denoted by the doubled lines. (b) The defect consists of two sites with A and B sublattice (the red and blue dot), forming an effective local pseudospin moment (the thick arrow in the shaded region). The bath fermions then screen the effective local momentum, resulting in a pseudospin Kondo singlet.

magnetic scattering is no longer necessary for generating Kondo behavior when gauge fluctuations come into play. More importantly, since the emergent Kondo features are direct consequences of gauge fluctuations, they can serve as promising indicators for QSLs. Our work therefore opens an unprecedented avenue to explore many-body resonances with new mechanisms, which may unveil the mysteries of the emergent gauge fluctuations in QSLs.

Chern-Simons representation of flux phases.—We first derive the flux phases from the spin-1/2 *XXZ* model based on the Chern-Simons (CS) representation [30–36], which will facilitate the study of the impurity problem.

The spin raising and lowering operators are statistically equivalent to hardcore bosons. To avoid the hardcore condition, we represent the spin operators by spinless fermions. Moreover, in order to ensure the bosonic statistics, a flux quanta has to be attached to each fermion, as shown by Fig. 2(a). This constitutes an exact representation of the spin excitations (see Supplemental Material [37]).

The attachment of a flux quanta can be achieved by coupling a CS gauge field A_μ [30] to the fermions, with the action

$$S_{CS} = \frac{1}{4\pi} \int d^2 x dt \epsilon^{\mu\nu\rho} A_\mu \partial_\nu A_\rho, \tag{1}$$

which is a pure gauge theory that has no contribution to the system energy [14].

We now consider a fermion hopping from $\mathbf{r}$ to $\mathbf{r}'$ on the honeycomb lattice as an example. An additional phase will be generated during the hopping, namely, $A_{\mathbf{r},\mathbf{r}'} = \int_{\mathbf{r}}^{\mathbf{r}'} d\mathbf{r}'' \cdot \mathbf{A}(\mathbf{r}'')$, where $\mathbf{A}(\mathbf{r})$ is the spatial component of A_μ. Moreover, the flux in any plaquette can be rigorously obtained by the contour integral as [37]
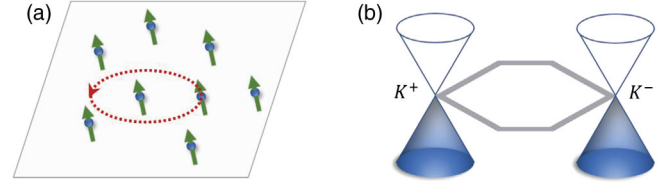

FIG. 2. The flux attachment and emergent flux phase. (a) The CS representation of the spin excitations. Each spinless fermion is attached to a flux quanta, reproducing the SU(2) algebra of the spin operators. (b) On honeycomb lattice, the saddle point solution is obtained, i.e., the flux phase with 2π flux in each hexagon. This state exhibits low-energy Dirac fermions with the valley degrees of freedom K^+ and K^-.

$$\phi_{\mathbf{r}} = \oint d\mathbf{r}'' \cdot \mathbf{A}(\mathbf{r}'') = 2\pi n_{\mathbf{r}}. \tag{2}$$

Hereby, we have labeled the plaquette by its bottom-left site $\mathbf{r}$. Equation (2) constitutes a flux condition in the CS fermion representation, which requires that the flux in the $\mathbf{r}$ plaquette be proportional to the local fermion number.

Using the above formalism, the *XXZ* model can be fermionized as $H = H_0 + H_{\text{int}}$ [37], where

$$H_0 = \sum_{\mathbf{r},\mathbf{r}'} (t_{\mathbf{r},\mathbf{r}'} f_{\mathbf{r}}^\dagger e^{iA_{\mathbf{r},\mathbf{r}'}} f_{\mathbf{r}'} + \text{H.c.}) \tag{3}$$

comes from the *XY* term, and $H_{\text{int}} = \sum_{\mathbf{r},\mathbf{r}'} u_{\mathbf{r},\mathbf{r}'} (n_{\mathbf{r}} - 1/2)(n_{\mathbf{r}'} - 1/2)$ is the local interaction arising from the Ising term. We note that H has particle-hole symmetry.

The gauge field in Eqs. (1) and (3) has fluctuations. However, for stable flux phases, the gauge fluctuations are irrelevant [51] in the sense that they only provide a flux background that modulates the energy of fermions [37,51]. Then, Eq. (3) is reduced to the exact flux model investigated by Lieb [10]. It was proved that the saddle point of Eq. (3) corresponds to the 2π-flux phase [10], where $\phi_{\mathbf{r}} = 2\pi \pmod{2\pi}$ in all the hexagons. Moreover, H_{int} is found irrelevant for $u_{\mathbf{r},\mathbf{r}'} \lesssim t_{\mathbf{r},\mathbf{r}'}$. Correspondingly, as shown by Fig. 2(b), two low-energy Dirac fermions emerge, located at $\mathbf{K}^a$ in momentum space, with the valley index $a = \pm$, i.e.,

$$H_0 = v_F \int \frac{d^2 k}{(2\pi)^2} f_{\mathbf{k},\alpha}^{(a)\dagger} \boldsymbol{\sigma}_{\alpha\beta}^{(a)} \cdot \mathbf{k} f_{\mathbf{k},\beta}^{(a)}, \tag{4}$$

where the sum of repeated indices is understood. $\boldsymbol{\sigma}^{(a)}$ is the Pauli matrix defined in the pseudospin (sublattice) space and is generally valley dependent. Equation (4) together with Eq. (1) concisely describes the flux phases under the CS representation, as long as they are stabilized.

Local gauge fluctuations excited by defect.—We now consider the bond defect, with the hopping $\epsilon < t$ and t the nearest-neighbor (NN) hopping. The Hamiltonian in Eq. (3) still respects the particle-hole symmetry, as well as
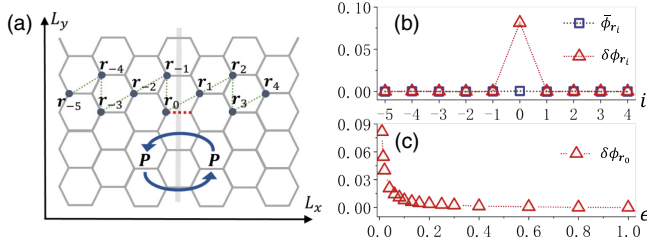
FIG. 3.   The effect of the bond defect on the flux phase. (a) The quenched bond is placed at the center of an 8×10 lattice. The system respects the reflection symmetry $\mathbf{P}$. (b) $\bar{\phi}_{\mathbf{r}}$ and $\delta\phi_{\mathbf{r}}$ obtained by the gradient descendant method (see Supplemental Material [37]). The expectations are evaluated with 200 random initial flux configurations. The x axis denotes the ten plaquettes along the dashed trajectory in (a), from the $\mathbf{r}_{-5}$ to $\mathbf{r}_4$. The $\mathbf{r}_0$ plaquette is the one adjacent to the quenched bond, whose hopping is taken as $\epsilon = 0.01$. (c) $\delta\phi_{\mathbf{r}_0}$ as a function of ϵ. The NN hopping is taken as $t = 1$.

a reflection symmetry with respect to the bond center $\mathbf{P}$, as shown by Fig. 3(a). In this case, Lieb's theorem is applicable, which states that the 2π flux is maintained in the plaquettes that intersect $\mathbf{P}$ [10].

So far, we have neglected the gauge fluctuations, which are irrelevant for flux phases stabilized on perfect lattices. Since a defect is now involved, the gauge fluctuations need to be considered more carefully. As indicated by Fig. 1(a), for $\epsilon \to 0$, the two hexagons sharing the bond become connected, forming a doubled plaquette. Then, opposite fluctuations $+\delta\phi$ and $-\delta\phi$ can naturally emerge in each of the two hexagons. Thus, a sufficiently strong bond defect with $\epsilon \ll t$ is expected to locally enhance the gauge fluctuations.

To verify the above expectation, we perform a self-consistent calculation on a finite lattice [37], with the fluxes treated as variational parameters. We start from initial states with randomly generated fluxes and optimize them by minimizing the system energy. Fast convergence to 2π flux is observed for most plaquettes. However, for $\epsilon \ll t$, it is found that the fluxes at the defect site $\delta\phi_{\mathbf{r}_0}$ can hardly converge, and they display a dependence on the initial states. Such numerical fluctuations essentially reflect the strong gauge fluctuations around the saddle point. To describe the fluctuation, we define $\bar{\phi}_{\mathbf{r}} = \langle \phi_{\mathbf{r}} \rangle$ and $\delta\phi_{\mathbf{r}} = (\langle \phi_{\mathbf{r}}^2 \rangle - \langle \phi_{\mathbf{r}} \rangle^2)^{1/2}$, where $\langle \ldots \rangle$ denotes the expectation over the random initial states. Clearly, $\bar{\phi}_{\mathbf{r}}$ and $\delta\phi_{\mathbf{r}}$ are numerical simulations of the saddle point fluxes and the gauge fluctuations, respectively.

We calculate $\bar{\phi}_{\mathbf{r}}$ and $\delta\phi_{\mathbf{r}}$ along the dashed trajectory in Fig. 3(a). As shown in Fig. 3(b), $\bar{\phi}_{\mathbf{r}}$ converges to 2π (gauge equivalent to 0) for all the plaquettes. Moreover, although $\delta\phi_{\mathbf{r}} = 0$ is obtained for most plaquettes, $\delta\phi_{\mathbf{r}_0}$ exhibits a significant fluctuation. In addition, as shown by Fig. 3(c), $\delta\phi_{\mathbf{r}_0}$ first changes slowly with decreasing ϵ and then grows fast for $\epsilon \ll t$, implying that only a strong defect can enhance the local gauge fluctuations.

The above numerical results reveal two important facts. First, the saddle point of Eq. (3) is still the 2π-flux phase, even if a bond defect is taken into account, in accordance with Lieb's theorem [10]. Second, the defect further enables local gauge fluctuations around the saddle point, in the plaquettes nearby the defect, consistent with the intuitive picture illustrated by Fig. 1(a).

Let us now focus on the defect site $\mathbf{r}_0$. The $\mathbf{r}_0$ plaquette has the saddle point flux 2π (mod 2π), as was proved by both Lieb's theorem and the self-consistent calculations. Moreover, we recall that the flux must be bound to the fermion number according to Eq. (2). Therefore, a local constraint at $\mathbf{r}_0$ is obtained, namely, $n_{\mathbf{r}_0} = n_{\mathbf{r}_0,A} + n_{\mathbf{r}_0,B} = 0, 1, 2$. Then, the particle-hole symmetry further fixes a single-occupation constraint condition [37], $n_{\mathbf{r}_0,A} + n_{\mathbf{r}_0,B} = 1$. Thus, the site $\mathbf{r}_0$ can only be occupied by a single fermion with pseudospin A or B. An effective impurity therefore emerges, displaying a pseudospin-1/2 moment, as indicated by Fig. 1(b). In order to facilitate the following analysis and distinguish the impurity fermions from the rest, we introduce the notation $d_{\mathbf{r}_0,\alpha} = f_{\mathbf{r}_0,\bar{\alpha}}$. Then, the single-occupation condition is cast into the simple form

$$\sum_\alpha d_{\mathbf{r}_0,\alpha}^\dagger d_{\mathbf{r}_0,\alpha} = 1. \tag{5}$$

In addition to Eq. (5), we have also shown that the fluctuation $\delta\phi_{\mathbf{r}_0}$ around the saddle point has to be taken into account for $\epsilon \ll t$. This can be equivalently written into local hoppings between the impurity states ($d_{\mathbf{r}_0,\alpha}$) and the bath fermions ($f_{\mathbf{r},\alpha}$), i.e.,

$$H^{\text{loc}} = \sum_{\mathbf{r},\alpha} t_{\mathbf{r},\mathbf{r}_0} f_{\mathbf{r},\alpha}^\dagger e^{iA_{\mathbf{r},\mathbf{r}_0}} d_{\mathbf{r}_0,\alpha} + \text{H.c.}, \tag{6}$$

where the CS gauge field $A_{\mathbf{r},\mathbf{r}_0}$ participates in the hopping processes. The sum here involves four local terms, as indicated by the double-lined bonds in Fig. 1(a).

Gauge field-induced pseudospin Kondo model.—So far, we have rigorously derived an effective model for $\epsilon \to 0$, which consists of a pseudospin-1/2 impurity ($d_{\mathbf{r}_0,\alpha}$) and a thermal bath ($f_{\mathbf{r},\alpha}$). The bath, in essence, is a 2π-flux phase with two vacancies at $\mathbf{r}_0$. It is thus described by

$$H^{\text{bath}} = v_F \int \frac{d^2k}{(2\pi)^2} f_{\mathbf{k},\alpha}^{(a)\dagger} \boldsymbol{\sigma}_{\alpha\beta}^{(a)} \cdot \mathbf{k} f_{\mathbf{k},\beta}^{(a)} + V f_{\mathbf{r}_0,\alpha}^\dagger f_{\mathbf{r}_0,\alpha}, \tag{7}$$

where the strong local potential V efficiently removes the two sites at $\mathbf{r}_0$ [52].

As discussed, the bath fermions are coupled to the effective impurity via Eq. (6), which includes the local CS gauge field $A_{\mathbf{r},\mathbf{r}_0}$. It is well known that the gauge field can mediate the electron-electron interaction in quantum electrodynamics. By analogy, here, the local CS gauge field

$A_{\mathbf{r},\mathbf{r}_0}$ will induce a local interaction between the bath and impurity. We therefore integrate out the local gauge fluctuations in Eqs. (1) and (6). In the continuum limit, a four-fermion term is generated as [37]

$$\delta H = J_{\mathrm{eff}} \sum_\alpha f^\dagger_{\mathbf{r}_0,\alpha} f_{\mathbf{r}_0,\bar\alpha} d^\dagger_{\mathbf{r}_0,\bar\alpha} d_{\mathbf{r}_0,\alpha}. \tag{8}$$

Clearly, this describes the pseudospin-flip processes when the bath fermions ($f_{\mathbf{r},\alpha}$) are scattered by the impurity ($d_{\mathbf{r}_0,\alpha}$). The gauge fluctuations here act as a "strong glue," and the resultant coupling constant J_{eff} is found to dominate over the energy scale of the Dirac fermions described by H^{bath}.

We observe a great similarity between Eq. (8) and the SU(2) Coqblin-Schrieffer model [53]. Indeed, after introducing the SU(2) generator, $X_{\alpha\beta} = d^\dagger_\alpha d_\beta - \delta_{\alpha\beta}/2$, and $X_{12} \sim S^+$, $X_{21} \sim S^-$, Eq. (8) along with the single-occupation condition in Eq. (5) is exactly mapped to the pseudospin exchange interaction,

$$H_K = J_{\mathrm{eff}} \mathbf{S}_p \cdot (f^\dagger_{\mathbf{r}_0,\alpha} \boldsymbol\sigma_{\alpha\beta} f_{\mathbf{r}_0,\beta}), \tag{9}$$

where $\mathbf{S}_p = (S_x, S_y)$ is the effective pseudospin-1/2 operator at $\mathbf{r}_0$. Since only (S_x, S_y) is present, the interaction H_K is highly anisotropic.

We have finally arrived at the low-energy effective theory for the renowned flux phases with a strong bond defect, i.e., Eqs. (7) and (9). Interestingly, an anisotropic pseudospin Kondo model emerges on top of the Dirac fermions with two valleys and a strong local potential V.

Asymmetric Kondo fixed point.—Equations (7) and (9) are similar in their form to the Kondo problems in Dirac semimetals or graphene [22–28]. However, there are several key distinctions. First, the bath is composed of effective fermions deconfined from the original quantum spin model. They neither carry charge nor spin, but pseudospin. Second, the bath fermions exhibit a pseudospin-momentum locking, as explicit in Eq. (7). Their pseudospins are therefore fully polarized. Third, the exchange interaction in Eq. (9) is not SU(2) invariant, but highly anisotropic with only the XY coupling. Last, the potential scattering V and the pseudospin exchange J_{eff} simultaneously take place in Eqs. (7) and (9). Thus, the interplay between them is non-negligible [28].

We first perform a RG analysis, treating V and J_{eff} as perturbations (see Supplemental Material [37]). To two-loop order, the RG flow is obtained as $dJ_{\mathrm{eff}}/dl = -J_{\mathrm{eff}} + J^2_{\mathrm{eff}} - J^3_{\mathrm{eff}}/2$ and $dV/dl = -V$. Both V and J_{eff} are irrelevant, flowing to the local momentum (LM) fixed point with $(V, J_{\mathrm{eff}}) = (0,0)$, as shown by the blue dot in Fig. 4(a).

The above perturbative RG flow breaks down for large V and J_{eff}, and is therefore not applicable to the current case. For large V and J_{eff}, we identify a stable AK fixed [54,55] with $(V, J_{\mathrm{eff}}) = (\infty, \infty)$, based on the duality between the
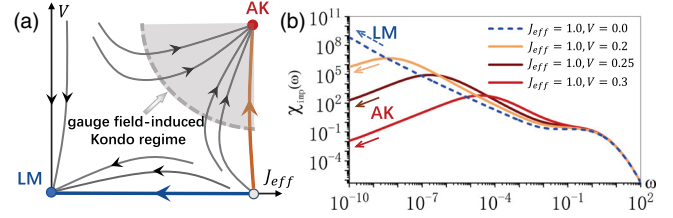

FIG. 4. The fixed points of the effective theory. (a) The LM and AK fixed point are found, together with a third unstable fixed point with $(V, J_{\mathrm{eff}}) = (0, \infty)$. The gauge field assisted Kondo model lies in a basin of attraction governed by the AK fixed point, as indicated by the shaded regime. (b) The NRG results of the imaginary part of the dynamical spin susceptibility $\chi_{\mathrm{imp}}(\omega)$. The system always flows to the LM fixed point for $V = 0$, corresponding to the horizontal blue RG trajectory in (a). The Fermi liquid behavior with $\chi_{\mathrm{imp}}(\omega) \propto \omega$ is found for finite V and large J_{eff}, justifying the flow to the AK fixed point in correspondence to the thick orange trajectory in (a).

strong-coupling Kondo model and the weak-coupling Anderson model [4,38]. By investigating the RG flow of the dual Anderson model, the fixed points far away from $(V, J_{\mathrm{eff}}) = (0,0)$ can be derived [37], producing the complete RG flow as shown by Fig. 4(a). Interestingly, since this emergent Kondo problem is characterized by large V and J_{eff}, the system is always located in the "basin of attraction" of the AK fixed point, as indicated by the shaded regime in Fig. 4(a).

The AK fixed point naturally arises as a result of the interplay between V and J_{eff}. For $V = 0$, J_{eff} is always irrelevant due to the vanishing density of states (DOS) at the Dirac point. The scattering V, in a sense, acts as a local chemical potential and enhances the local DOS (LDOS), which in turn favors the Kondo screening. We further perform a full-density matrix numerical renormalization group (NRG) calculation [37,39,40]. Figure 4(b) shows the calculated dynamical spin susceptibility $\chi_{\mathrm{imp}}(\omega)$ for different V with $J_{\mathrm{eff}} = 1$. In low energy, the calculated $\chi_{\mathrm{imp}}(\omega)$ displays the scaling $\chi_{\mathrm{imp}}(\omega) \propto \omega$ for $V \neq 0$, implying the occurrence of the Fermi liquid behavior from the Kondo fixed point. Therefore, the system flows to the AK (LM) fixed point for $V \neq 0$ ($V = 0$), consistent with the thick orange (blue) RG trajectory in Fig. 4(a).

So far, all the results are obtained for a short-range coupling J_{eff}. If one assumes a long-range $|\mathbf{r}|$ dependence of $J_{\mathrm{eff}}(|\mathbf{r}|)$, then the intervalley scattering amplitude will become smaller compared to the intravalley one. In this case, the two-channel Kondo physics can be relevant [37,41], resulting in the non-Fermi-liquid fixed point as well as the crossover between the Fermi liquid and non-Fermi-liquid behavior.

Conclusion and discussion.—The predicted Kondo behavior exhibits several unique features that are experimentally measurable. First, although the local Kondo resonance arises from an unusual mechanism, it will still

exhibit a LDOS peak near the Fermi energy. The scanning tunneling microscopy and spectroscopy measurements may be applicable for measuring the impurity LDOS. Second, since the screening is formed by deconfined and chargeless excitations rather than electrons, the characteristic resistivity behavior of the conventional Kondo effect does not take place here. Third, the nature of fixed points can be manifested by thermal transport [42,43]. We have calculated the thermal conductivity $\sigma_E(T)/T$ at low energy scales near the AK fixed point based on the conformal field theory [41,44–49,56]. It is found that $\sigma_E(T)/T$ scales as $\sigma_E(T)/T \sim T^2$ at low temperatures [37]. Moreover, it is known that the potential scattering V can bring about significant deviations from the universal scaling at higher temperatures ($T \gtrsim T_K$, with T_K the Kondo temperature) [42,57]. Therefore, a nonmonotonous temperature dependence of the thermal conductivity is expected. Last, because of the pseudospin-momentum locking of the bath, both the pseudospin and the orbital angular momentum will participate in the screening process. This always leads to an anisotropic pseudospin correlation, which has been proved by Ref. [50] in the context of topological superconductors.

This Letter reveals a gauge-fluctuation-induced Kondo behavior. The Kondo screening here is caused by gauge fluctuations and therefore has a fundamentally different origin from the conventional Kondo effect. Nevertheless, it provides a promising indicator for identifying QSLs. These results are generalizable to flux phases stabilized on different lattices and other physical systems (see Supplemental Material [37]). Particularly, the fermions coupled to stable gauge fluxes can also emerge from interacting bosonic systems with degenerate single-particle dispersions [58–60], e.g., the dilute atomic gases [61]. Furthermore, it is highly desirable to verify our theory by large-scale numerical simulations. For example, the quantum Monte Carlo calculations may be applied if the sign problem can be avoided in some flux phases [62].

[*]rwang89@nju.edu.cn
[†]bgwang@nju.edu.cn

[1] J. Kondo, Prog. Theor. Phys. 32, 37 (1964).
[2] K. G. Wilson, Rev. Mod. Phys. 47, 773 (1975).
[3] N. Andrei, Phys. Rev. Lett. 45, 379 (1980).
[4] A. C. Hewson, The Kondo Problem to Heavy Fermions (Cambridge University Press, Cambridge, England, 1993).
[5] P. Nozières, J. Low Temp. Phys. 17, 31 (1974).
[6] P. W. Anderson, Mater. Res. Bull. 8, 153 (1973).
[7] L. Savary and L. Balents, Rep. Prog. Phys. 80, 016502 (2017).
[8] P. W. Anderson, Science 235, 1196 (1987).
[9] N. Read and S. Sachdev, Phys. Rev. B 42, 4568 (1990).
[10] E. H. Lieb, Phys. Rev. Lett. 73, 2158 (1994).
[11] M. U. Ubbens and P. A. Lee, Phys. Rev. B 46, 8434 (1992).
[12] S. Gazit, M. Randeria, and A. Vishwanath, Nat. Phys. 13, 484 (2017).
[13] X.-G. Wen, Phys. Rev. B 65, 165113 (2002).
[14] G. V. Dunne, Aspects of Chern-Simons Theory, arXiv:hep-th/9902115.
[15] M. Gomilšek, R. Žitko, M. Klanjšek, M. Pregelj, C. Baines, Y. Li, Q. M. Zhang, and A. Zorko, Nat. Phys. 15, 754 (2019).
[16] G. Chen and J. L. Lado, Phys. Rev. Research 2, 033466 (2020).
[17] A. Tanaka and X. Hu, Phys. Rev. Lett. 95, 036402 (2005).
[18] C. Wang, A. Nahum, M. A. Metlitski, C. Xu, and T. Senthil, Phys. Rev. X 7, 031051 (2017).
[19] A. Thomson and S. Sachdev, Phys. Rev. X 8, 011012 (2018).
[20] X.-Y. Song, C. Wang, A. Vishwanath, and Y.-C. He, Nat. Commun., 10, 4254 (2019).
[21] T. C. Hsu, J. B. Marston, and I. Affleck, Phys. Rev. B 43, 2866 (1991).
[22] D. Ma, H. Chen, H. Liu, and X. C. Xie, Phys. Rev. B 97, 045148 (2018).
[23] H.-B. Zhuang, Q.-f. Sun, and X. C. Xie, Europhys. Lett. 86, 58004 (2009).
[24] J.-H. Chen, L. Li, W. G. Cullen, E. D. Williams, and M. S. Fuhrer, Nat. Phys. 7, 535 (2011).
[25] B. Uchoa, T. G. Rappoport, and A. H. Castro Neto, Phys. Rev. Lett. 106, 016801 (2011).
[26] T.-F. Fang, W. Zuo, and H.-G. Luo, Phys. Rev. Lett. 101, 246805 (2008).
[27] L. Li, Jin-H. Sun, Z.-H. Wang, D.-H. Xu, H.-G. Luo, and W.-Q. Chen, Phys. Rev. B 98, 075110 (2018).
[28] A. K. Mitchell and L. Fritz, Phys. Rev. B 92, 121109(R) (2015).
[29] R. Zheng, R.-Q. He, and Z.-Y. Lu, Chin. Phys. Lett. 35, 067301 (2018).
[30] A. López, A. G. Rogo, and E. Fradkin, Phys. Rev. B 49, 15139 (1994).
[31] K. Yang, L. K. Warman, and S. M. Girvin, Phys. Rev. Lett. 70, 2641 (1993).
[32] R. Wang, B. Wang, and T. A. Sedrakyan, Phys. Rev. B 98, 064402 (2018).
[33] T. A. Sedrakyan, V. M. Galitski, and A. Kamenev, Phys. Rev. B 95, 094511 (2017).
[34] T. A. Sedrakyan, R. Moessner, and A. Kamenev, Phys. Rev. B 102, 024430 (2020).
[35] T. A. Sedrakyan, L. I. Glazman, and A. Kamenev, Phys. Rev. Lett. 114, 037203 (2015).
[36] R. Wang, B. Wang, and T. Sedrakyan, arXiv:2010.10067.

[37] See Supplemental Materials http://link.aps.org/supplemental/10.1103/PhysRevLett.127.237202 for pertinent technical details on relevant proofs and derivations, which includes Refs. [4,10,34,38–50].

[38] Q. L. Li, R. Wang, K. X. Xie, X. X. Li, C. Zheng, R. X. Cao, B. F. Miao, L. Sun, B. G. Wang, and H. F. Ding, Phys. Rev. B **97**, 155401 (2018).

[39] A. Weichselbaum and J. von Delft, Phys. Rev. Lett. **99**, 076402 (2007).

[40] A. Weichselbaum, Ann. Phys. (Amsterdam) **327**, 2972 (2012).

[41] I. Affleck and A. W. W. Ludwig, Nucl. Phys. **B360**, 641 (1991).

[42] A. Kiss, Y. Kuramoto, and S. Hoshino, Phys. Rev. B **84**, 174402 (2011).

[43] C. P. Moca, A. Roman, and D. C. Marinescu, Phys. Rev. B **83**, 245308 (2011).

[44] I. Affleck and A. W. W. Ludwig, Nucl. Phys. **B352**, 849 (1991).

[45] I. Affleck and A. W. W. Ludwig, Phys. Rev. Lett. **67**, 161 (1991).

[46] A. W. W. Ludwig and I. Affleck, Phys. Rev. Lett. **67**, 3160 (1991).

[47] I. Affleck, A. W. W. Ludwig, H-B. Pang, and D. L. Cox, Phys. Rev. B **45**, 7918 (1992).

[48] I. Affleck and A. W. W. Ludwig, Phys. Rev. B **48**, 7297 (1993).

[49] A. W. W. Ludwig and I. Affleck, Nucl. Phys. **B428**, 545 (1994).

[50] R. Wang, W. Su, J.-X. Zhu, C. S. Ting, H. Li, C. Chen, B. Wang, and X. Wang, Phys. Rev. Lett. **122**, 087001 (2019).

[51] M. Hermele, T. Senthil, M. P. A. Fisher, P. A. Lee, N. Nagaosa, and X.-G. Wen, Phys. Rev. B **70**, 214437 (2004).

[52] V. M. Pereira, J. M. B. Lopes dos Santos, and A. H. Castro Neto, Phys. Rev. B **77**, 115109 (2008).

[53] B. Coqblin and J. R. Schrieffer, Phys. Rev. **185**, 847 (1969).

[54] C. Gonzalez-Buxton and K. Ingersent, Phys. Rev. B **57**, 14254 (1998).

[55] L. Fritz and M. Vojta, Rep. Prog. Phys. **76**, 032501 (2013).

[56] E. Witten, Commun. Math. Phys. **92**, 455 (1984).

[57] J. Kondo, Phys. Rev. **169**, 437 (1968).

[58] T. A. Sedrakyan, V. M. Galitski, and A. Kamenev, Phys. Rev. Lett. **115**, 195301 (2015).

[59] T. A. Sedrakyan, L. I. Glazman, and A. Kamenev, Phys. Rev. B **89**, 201112(R) (2014).

[60] S. Maiti and T. Sedrakyan, Phys. Rev. B **99**, 174418 (2019).

[61] J. R. Anglin and W. Ketterle, Nature (London) **416**, 211 (2002).

[62] X. Y. Xu, Y. Qi, L. Zhang, F. F. Assaad, C. Xu, and Z. Y. Meng, Phys. Rev. X **9**, 021022 (2019).